ACS APPLIED MATERIALS & INTERFACES

www.acsami.org Research Article

High-Mobility IZO Thin-Film Transistors Enabled by Precise Hydrogen Control Using a $SiO_2-Al_2O_3$ Supercycle via Plasma-Enhanced Atomic Layer Deposition

Sunghwan Park, Seong-In Cho, Hwa Young Kim, Sang-Hee Ko Park,* and Jong Beom Ko*

Cite This: https://doi.org/10.1021/acsami.5c12926 Read Online

ACCESS | Metrics & More | Article Recommendations | Supporting Information

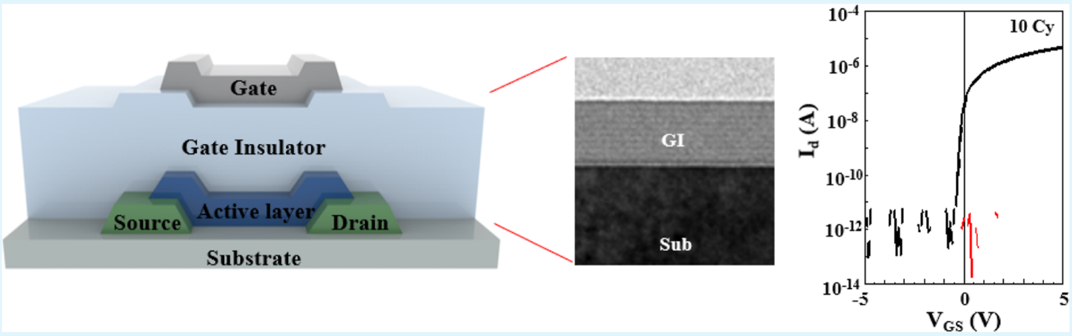

ABSTRACT: A precise strategy to control hydrogen incorporation is essential for achieving high-performance oxide thin-film transistors (TFTs) as hydrogen plays a key role in tuning carrier concentration and passivating defect states. In this study, we report a top-gate oxide thin-film transistor structure that utilizes a plasma-enhanced atomic layer deposition (PEALD) supercycled $SiO_2-Al_2O_3$ gate insulator (GI), enabling precise hydrogen control through a tunable layering sequence. Hydrogen incorporation into the active channel is modulated with precise control by varying the number of hydrogen-rich SiO_2 subcycles. Comprehensive analyses reveal that moderate hydrogen incorporation effectively passivates oxygen-related defects while introducing shallow donor states, enhancing mobility, and suppressing charge trapping. The optimized device with ten cycles of H-rich SiO_2 exhibits a high field-effect mobility of 47.4 $cm^2/V{\cdot}s$, a turn-on voltage (V_{on}) of −0.46 V, a subthreshold swing of 71.3 mV/dec and negligible hysteresis, an on/off current ratio of $\sim10^7$, and superior bias stability under positive and negative stress conditions. In contrast, excess hydrogen from 15 cycles leads to the loss of switching behavior caused by the intermixing of GI layers, resulting in uncontrolled hydrogen diffusion and excessive carrier generation. These results demonstrate that the PEALD supercycle process offers a reliable strategy for hydrogen modulation in oxide semiconductors, enabling an optimized trade-off between mobility and stability in high-performance TFTs.

KEYWORDS: *oxide thin-film transistor, atomic layer deposition, hydrogen, defect passivation, high mobility, gate insulator, super cycle*

1. INTRODUCTION

Thin-film transistors (TFTs) utilizing oxide semiconductors (OSs) such as indium−gallium-zinc oxide (IGZO) were first reported by the Hosono group in 2004.[1] These devices gained significant attention in the display industry because of their high mobility and uniform electrical properties over large-area substrates, all achievable at a relatively low cost.[2,3] Compared to hydrogenated amorphous silicon TFTs, OS demonstrate superior field-effect mobility and remarkably low off-current levels.[4] Recently, OS emerged as a promising candidate for channel materials in the semiconductor industry; their moderate carrier mobility, extremely low off-current, and potential for three-dimensional integration make them suitable for nondisplay applications such as memories,[5−8] logic devices, next generation electronics, and complementary metal-oxide-semiconductor image sensors.[9] To meet the performance requirements of next generation electronics, high-resolution and large-area displays, OSs need to exhibit high electron mobility, low subthreshold swing (S.S), near zero turn on voltage (V_{on}), and low off-current.[10] Various OSs have been introduced, including InGaZnO (IGZO), InSnZnO (ITZO), and InZnO (IZO).[11−13] IZO is applied to various fields such as memory devices, display components, and neuromorphic devices because of its high mobility.[13−15] Notably, conventional sputtered amorphous IZO TFTs have demonstrated saturation mobilities exceeding 100 $cm^2/V{\cdot}s$, underscoring the material's potential for high-performance applications.[16] The

Received: July 1, 2025
Revised: October 29, 2025
Accepted: November 20, 2025

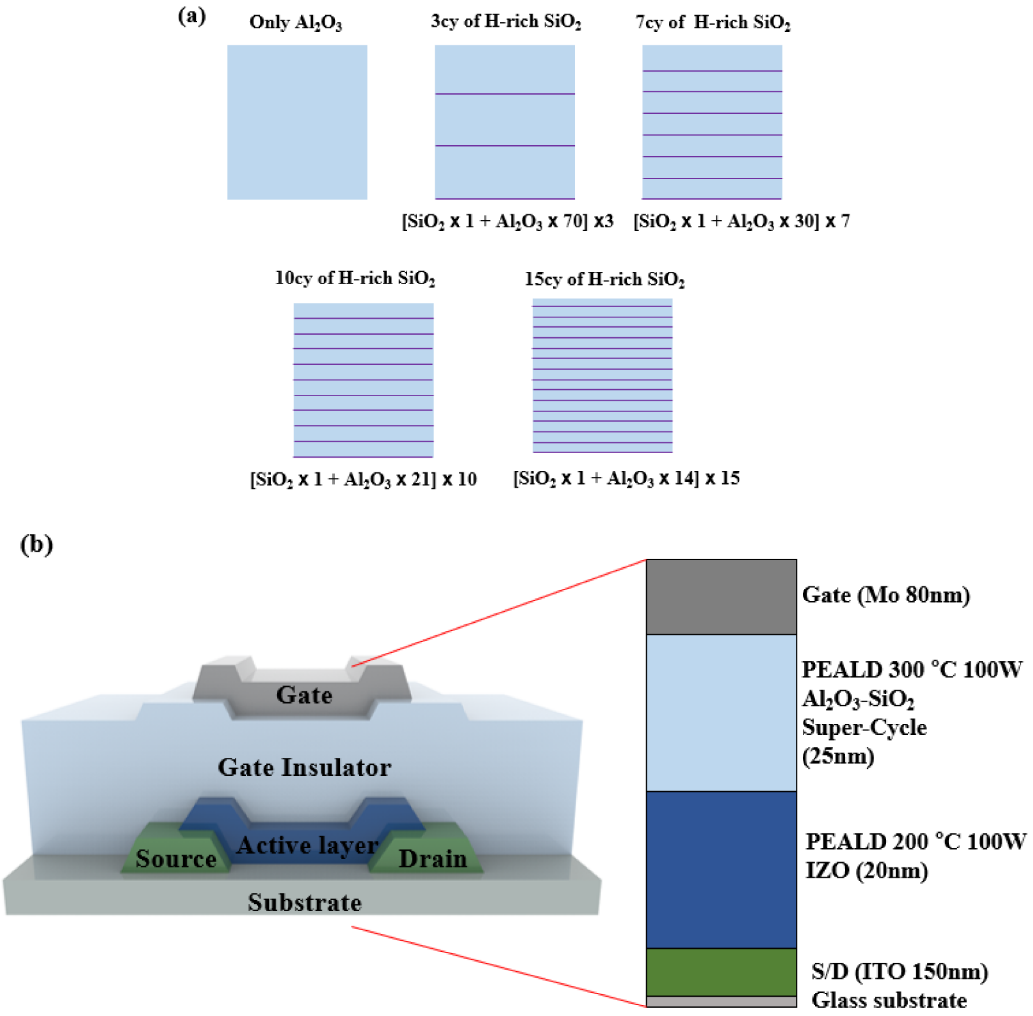

Figure 1. (a) Schematics of PEALD supercycle gate insulators with different H-rich SiO_2 cycles. (b) Schematic of a high-mobility TFT with a supercycle GI.

electrical properties of OSs are strongly affected by their stoichiometry, which optimizes their composition and can further enhance electron mobility.[17] In addition to compositional control, the structural design of the OS devices plays a crucial role. Among various oxide TFT structures, a self-aligned structure has been widely adopted in advanced oxide TFTs because it provides smaller overlap capacitance and reduced parasitic resistance−capacitance delay compared with the conventional bottom-gate structure, leading to faster switching and better scalability in high-resolution display applications.[18−20] The top-gate configuration, which can be implemented in a self-aligned manner, is therefore considered a promising architecture for realizing high-performance oxide TFTs. Nevertheless, in top-gate structures where the gate insulator (GI) is directly deposited on the active layer, the mobility and stability of oxide TFTs are highly affected by the GI fabrication process.[21−25] The channel surface exposed to excessive plasma conditions can suffer from interface damage, leading to large hysteresis and poor electrical stability despite otherwise excellent intrinsic electrical characteristics.[26] The GI/OS interface properties are particularly critical for achieving high performance and stability in oxide TFTs, especially for multicomponent dielectric systems.[27] Defects at the GI/OS interface, particularly oxygen-related defects such as oxygen interstitials (O_i) and oxygen vacancies (V_o) act as electron traps, which leads to performance degradation.[28−30] Plasma-enhanced atomic layer deposition (PEALD) offers precise control over GI properties, which reduces oxygen-related defects and hydrogen incorporation.[20] Optimizing PEALD conditions minimizes charge traps and donor concentrations, improving TFT reliability.[22] Moderate hydrogen incorporation from the GI into the active layer can enhance device performance by increasing free electron concentration and mobility.[25] In addition, hydrogen passivates defects at the GI/OS interface, which leads to improved Positive Bias Temperature Stress (PBTS) stability.[28,31−34] However, excessive hydrogen incorporation can have adverse effects, which causes a negative shift in the V_{on} and aggravates PBTS-induced degradation caused by the formation of an overabundance of shallow donors, destabilizing overall device stability.[25,35,36] This creates a trade-off between enhancing mobility and ensuring device stability, highlighting the need for optimized process conditions to balance these competing factors. Current methods to control hydrogen concentration, including modulating the deposition temperature of the GI or employing hydrogen plasma treatment,[37,38] lack the precision required for accurate control. High-mobility oxide TFTs possess higher intrinsic carrier concentrations, which makes them highly sensitive to hydrogen incorporation.[20,39] Precise hydrogen control is essential for ensuring both high mobility

https://doi.org/10.1021/acsami.5c12926

Table 1. GI Structures Engineered by Varying the Number of Supercycles

H-rich SiO_2 sub-cycles per super-cycle [cy]	Al_2O_3 cycles per supercycle [cy]	number of supercycles [cy]	total H-rich SiO_2 cycles [cy]	structure summary
0	210	1	0	only Al_2O_3
1	70	3	3	$[(SiO_2 \times 1) + (Al_2O_3 \times 70)] \times 3$
1	30	7	7	$[(SiO_2 \times 1) + (Al_2O_3 \times 30)] \times 7$
1	21	10	10	$[(SiO_2 \times 1) + (Al_2O_3 \times 21)] \times 10$
1	14	15	15	$[(SiO_2 \times 1) + (Al_2O_3 \times 14)] \times 15$

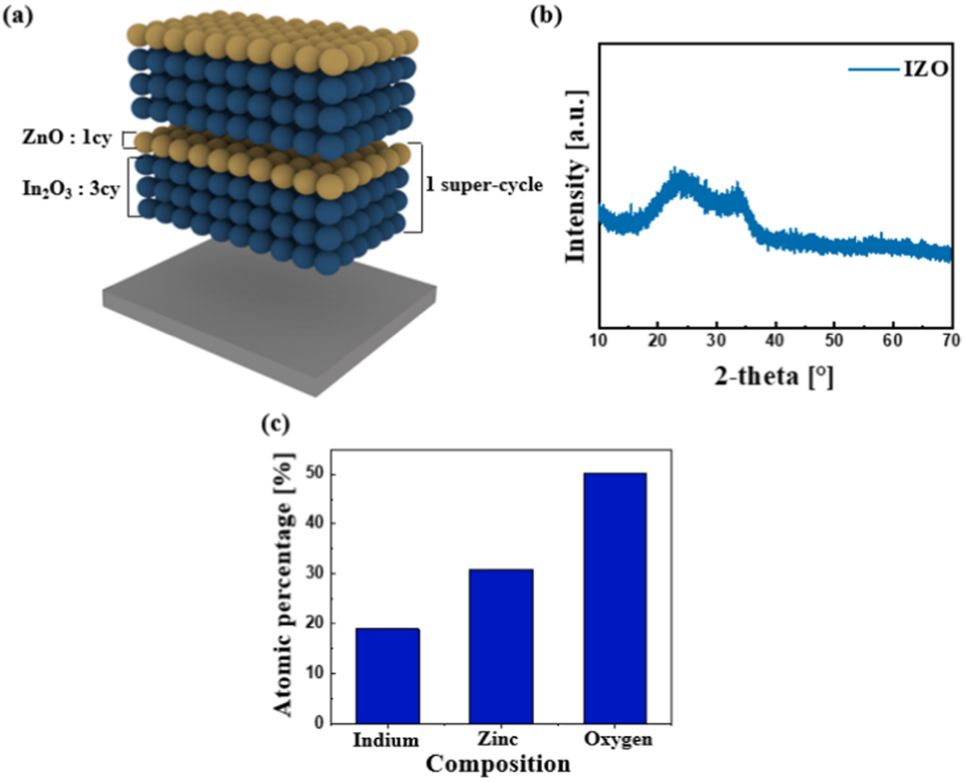

Figure 2. (a) Schematic illustration of the PEALD supercycle method for IZO thin-film deposition. (b) XRD result of the IZO thin film. (c) Atomic composition of IZO analyzed by XPS.

and device stability, and therefore, a new strategy for the delicate control of hydrogen in OSs is pivotal to achieving the dual goals of high mobility and high stability in oxide TFTs.

In this study, we developed a strategy to control hydrogen incorporation by engineering a GI with alternating hydrogen-rich and hydrogen-deficient layers. The top-gate structure allowed direct GI deposition on the channel, enabling precise hydrogen control at the GI/OS interface, which is essential for evaluating the effect of the supercycled GI. Top-gate oxide TFTs were fabricated using a PEALD supercycle process integrating hydrogen-rich SiO_2 and hydrogen-deficient Al_2O_3. The atomic-scaled H-rich SiO_2 layer containing ∼6.12 at % hydrogen functions as a hydrogen supplement layer for enabling the refined control of hydrogen incorporation through short O_2 plasma reactions during the PEALD process. The Al_2O_3 layer was deposited under high-temperature and optimized plasma conditions to achieve a low hydrogen content. Hydrogen concentration can be precisely controlled by modulating H-rich SiO_2 cycles in the PEALD process, which enables hydrogen diffusion into the active layer during the postannealing process. Comprehensive analyses confirm that moderate hydrogen incorporation effectively passivates defects and increases the carrier concentration, thereby leading to enhanced electrical performance and reliability. These findings indicate that precise hydrogen modulation is key to simultaneously achieving a high mobility and stability in oxide TFTs.

2. EXPERIMENTAL SECTION

Top-gate bottom-contact (TGBC) oxide TFTs were fabricated on glass substrates by using a sequential thin-film deposition and patterning process for investigating the effects of hydrogen incorporation via GI engineering. A 150 nm-thick InSnO (ITO) layer was deposited on the glass substrate to serve as a source/drain electrode. Then, a 20 nm-thick IZO semiconductor layer was deposited by PEALD at 200 °C using a supercycle process. The deposition was carried out using 3-(dimethylamino)propyl]-dimethylindium (DADI) as the indium precursor and diethylzinc (DEZ) as the zinc precursor, with 100 W RF O_2 plasma as the oxygen reactant. The PEALD method was employed to form a high-mobility IZO active layer in which In_2O_3 and ZnO atomic layers were alternately deposited. Each supercycle comprises three cycles of In_2O_3 followed by one cycle of ZnO $[(In_2O_3 \times 3) + (ZnO \times 1)]$.

Each PEALD subcycle was composed of the following steps:

In_2O_3 cycle: (1) DADI dose: 1.0 s (Ar 50 sccm), (2) Ar purge: 10.0 s, (3) RF O_2 plasma: 100 W for 2.0 s (O_2 500 sccm), and (4) Ar purge: 10.0 s.

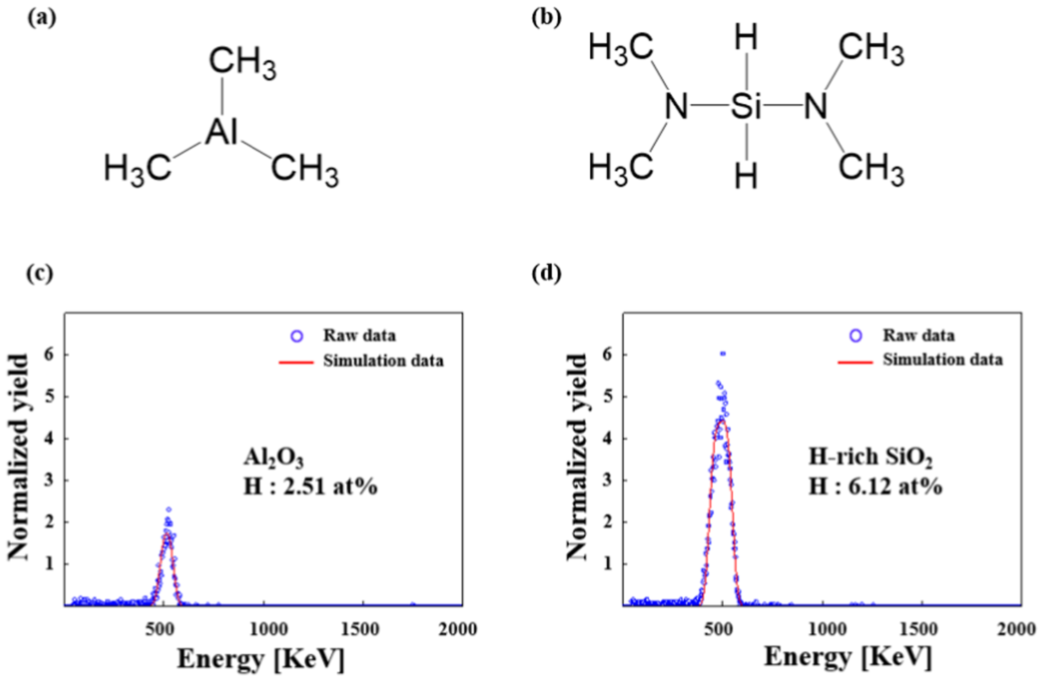

Figure 3. Schematic of precursor and adsorption of (a) trimethylaluminum (TMA) and (b) bis (diethylamino) silane (BDEAS). (c) H concentration (ERD) of Al_2O_3. (d) H concentration (ERD) of SiO_2.

ZnO cycle: (1) DEZ dose: 0. One s (Ar 500 sccm), (2) Ar purge: 10.0 s, (3) RF O_2 plasma: 100 W for 2.0 s (O_2 500 sccm), and (4) Ar purge: 10.0 s.

2.1. GI Formation.

At 300 °C, the Al_2O_3 layer is deposited via PEALD using trimethylaluminum (TMA) as the Al precursor with a 100 W oxygen plasma source. The SiO_2 layer is similarly deposited via PEALD using bis(diethylamino)silane (BDEAS, $H_2Si[N(C_2H_5)_2]_2$) as the Si precursor. The O_2 plasma exposure time during SiO_2 deposition is extremely shortened to enhance hydrogen incorporation, resulting in an incomplete precursor reaction and increased hydrogen content. Figure 1a shows that a series of GI structures was systematically designed by modulating the number of H-rich SiO_2 supercycles in the PEALD process to investigate the effect of hydrogen incorporation. The growth per cycle was approximately 0.112 nm for SiO_2 and 0.119 nm for Al_2O_3, giving a total GI thickness of ∼25 nm for all configurations. This constant thickness ensured sufficient capacitance for stable gate control while allowing precise modulation of the H-rich SiO_2 cycles in the supercycle structure. The detailed GI configurations, including the number of supercycles and the total H-rich SiO_2 cycles in each stack, are summarized in Table 1.

Each PEALD subcycle was composed of the following steps:

SiO_2 cycle: (1) BDEAS dose: 0.2 s (Ar 500 sccm), (2) Ar purge: 5.0 s, (3) RF O_2 plasma: 100 W for 0.3 s (O_2 500 sccm), and (4) Ar purge: 7.0 s.

Al_2O_3 cycle: (1) TMA dose: 0.2 s (Ar 500 sccm), (2) Ar purge: 5.0 s, (3) RF O_2 plasma: 100 W for 2.0 s (O_2 500 sccm), and (4) Ar purge: 7.0 s.

Finally, an 80 nm-thick Mo layer was deposited by DC sputtering to serve as the gate electrode. All thin films were patterned by using photolithography and chemical wet etching techniques. Postfabrication, vacuum annealing was conducted at 360 °C for 2 h for facilitating hydrogen diffusion and enhancing the electrical performance of the TFTs. The channel width and length of the active region were both 20 μm. The final device structure and fabrication process are presented in Figure 1b.

The electrical performance and bias stability of the fabricated TFTs were evaluated at room temperature under dark conditions to prevent photoinduced effects. Measurements were performed using an Agilent 4284A Precision LCR Meter and an HP 4156A Semiconductor Parameter, both integrated with a probe station. Interface analysis between the IZO channel and GI was performed using High resolution transmission electron microscopy (HRTEM), X-ray photoelectron spectroscopy (XPS), and Secondary ion mass spectrometry (SIMS) to clarify the mechanisms underlying the observed device behavior. The XPS measurements were conducted using a Thermo Scientific K-Alpha$^+$ system, and SIMS profiling was conducted using a CAMECA IMS-7f instrument on samples annealed under the same conditions as the TFTs, which enables the comparison of hydrogen-related species across different GI structures.

3. RESULTS AND DISCUSSION

Figure 2a presents a schematic of the IZO deposition sequence. Amorphous IZO is selected to enhance device performance because polycrystalline semiconductors often suffer from low mobility and poor uniformity owing to grain boundary defects.[40,41] In_2O_3 crystallizes in a bixbyite structure, whereas ZnO forms a wurtzite structure.[42] The 3:1 supercycle ratio was employed to ensure the deposition of amorphous IZO and minimize grain boundary-related defects. The X-ray diffraction (XRD) profiles in Figure 2b show the deposited IZO exhibited an amorphous phase, characterized by a broad hump near $2\theta \approx 32°$, which is indicative of amorphous IZO. The IZO film remained amorphous after GI deposition and postannealing (Figure S1, Supporting Information). The absence of sharp diffraction peaks corresponding to the (222), (400), and (440) planes, which usually appear at 2θ values of 30.6°, 35.5°, and 51.1°, respectively,[43] further confirms the amorphous nature of the IZO film. The atomic composition of the 20 nm-thick IZO layer measured by XPS was 19.96 atom % In, 30.01 atom % Zn, and 50.03 atom % O, as shown in Figure 2c. These IZO films served as the channel layer in TGBC TFTs with a channel width and length of 20 μm (width/length = 1).

Figure 3a,b shows the molecular structures of TMA and BDEAS, which are precursors for Al_2O_3 and SiO_2, respectively. BDEAS contains Si−H bonds that can serve as direct hydrogen sources under short plasma exposure, enabling hydrogen

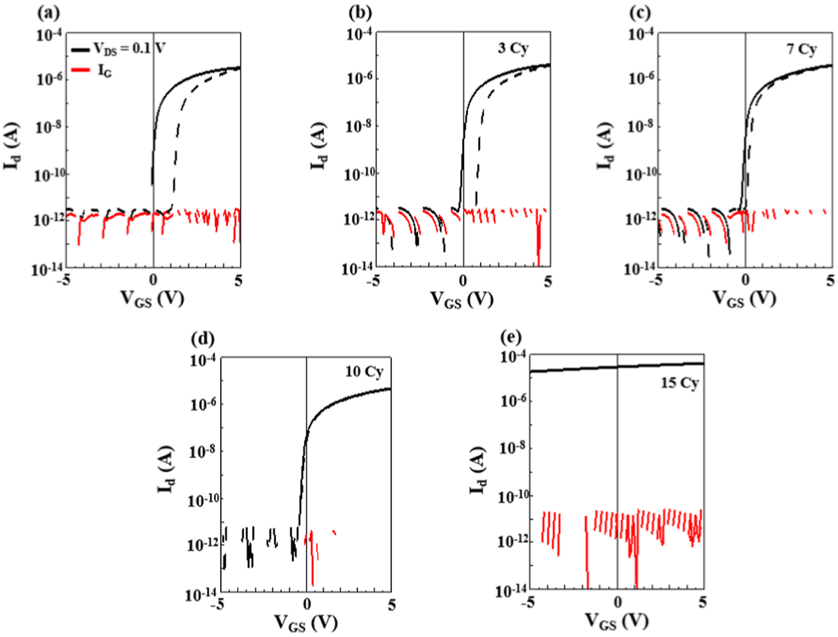

Figure 4. Transfer curves of TFTs with PEALD supercycle gate insulators: (a) with only Al_2O_3, (b) with 3 cycles of H-rich SiO_2, (c) with 7 cycles of H-rich SiO_2, (d) with 10 cycles of H-rich SiO_2, (e) with 15 cycles of H-rich SiO_2.

Table 2. Extracted Electrical Parameters (at V_d = 0.1 V) with Average and Standard Deviation Obtained from Measurements on 10 Devices with Different Cycles of H-Rich SiO_2 after Vacuum Annealing at 360 °C

cycles of H-rich SiO_2 [cy]	V_{on} [V]	μ_{lin} [$cm^2/(V\ s)$]	S.S [mV/dec]	hysteresis [V]
0 (only Al_2O_3)	−0.17 ± 0.06	28.02 ± 0.51	74.9 ± 12.0	1.13 ± 0.12
3	−0.18 ± 0.08	31.50 ± 0.99	72.9 ± 5.0	0.98 ± 0.08
7	−0.28 ± 0.04	40.32 ± 0.24	72.4 ± 2.0	0.28 ± 0.04
10	−0.46 ± 0.13	47.40 ± 0.61	71.3 ± 5.0	0
15		conductive		

incorporation into the GI. In contrast, TMA lacks such hydrogen-supplying bonds.[44] Figure 3c,d presents the elastic recoil detection (ERD) analysis results of Al_2O_3 and SiO_2 thin films, which reveal hydrogen concentrations of 2.2×10^{16} and 4.63×10^{16} atoms/cm^2, respectively. This result indicates that the hydrogen concentration in the SiO_2 film is more than twice that in the Al_2O_3 film. The presence of hydrogen in ALD films originates from the incomplete elimination of precursor ligands during the deposition process. The high deposition temperature and sufficient oxygen plasma in Al_2O_3 led to low hydrogen incorporation.[45] In contrast, the extremely short oxygen plasma exposure during PEALD for SiO_2 increased hydrogen content.[46] Plasma exposure time affects precursor reactivity, and therefore, in previous research, shorter exposure led to incomplete BDEAS precursor reaction, thereby resulting in higher hydrogen incorporation in H-rich SiO_2.[22] The fabricated GIs exhibit negligible carbon incorporation, as confirmed by the XPS depth profile (Figure S2) and SIMS depth profile (Figure S3). Furthermore, the elemental distribution across the active layer and GI regions remains consistent across different H-rich SiO_2 cycle conditions (Figure S2), confirming that the supercycle process does not induce bulk compositional variation.

As shown in Figure 4, the fabricated TGBC TFT devices exhibit distinct trends in electrical characteristics based on the number of H-rich SiO_2 cycles. The drain voltage (V_d) of 0.1 V was applied to TFTs (width/length = 20/20 μm) for measuring the transfer characteristics in the linear region. The solid and dashed lines represent forward and reverse sweeps, respectively. The V_d of 0.1 V was utilized to extract the field-effect mobility using the experimentally measured GI capacitance (C_i) for each GI stack (Figure S4) and the corresponding V_{on}. To confirm the onset of current saturation, the output characteristics of all devices and the transfer curve of the device with ten cycles of H-rich SiO_2 measured at V_d = 4.1 V are presented in Figure S5, showing that current saturation occurs at approximately 4 V. As shown in Figure S5e, the device with ten cycles of H-rich SiO_2 exhibits a typical transfer curve even in the saturation region, without any noticeable anomalies.

The transfer characteristics are analyzed for different supercycle numbers, and the extracted average values of electrical parameters for ten devices are summarized in Table 2. In the PEALD supercycle process, increasing the number of H-rich SiO_2 cycles from 0 to 10 resulted in incorporating hydrogen as a donor, which leads to a significant enhancement in mobility (μ_{lin}), thereby increasing from 28.02 to 47.4 cm^2/V·s. The underlying mechanism responsible for an increase of nearly twice in mobility needs to be analyzed in relation to V_{on} considering the number of H-rich SiO_2 cycles during the PEALD supercycle for GI deposition. A reasonable explanation involves hydrogen diffusion from different GIs during the deposition of Al_2O_3 and SiO_2 or subsequent postannealing. Hydrogen in the H-rich SiO_2 plays a crucial role, serving as both a defect passivator and shallow donor in OSs.[44,47] This combined effect contributes to enhanced mobility through (1)

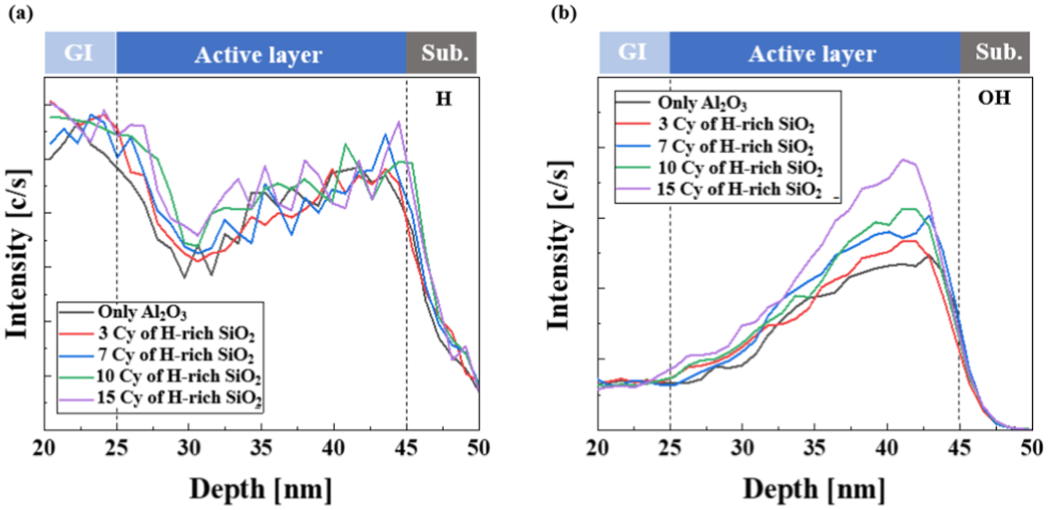

Figure 5. SIMS depth profiles of (a) H and (b) OH in the GI/active/substrate structure with different cycles of H-rich SiO_2.

an increase in carrier concentration via electron donation,[48,49] which exploits the percolation conduction mechanism characteristic of OSs,[4] and (2) passivation of electron trap sites, which effectively lowers barriers to electron flow and improves overall conductivity.[31−33] This improvement is accompanied by a negative shift in V_{on}, which shifts from −0.17 to −0.46 V, which is indicative of a trade-off between enhanced carrier transport and increased donor concentration. V_{on} exhibits a tendency to shift in the negative direction with an increase in the carrier concentration.[4] The devices with 15 cycles of H-rich SiO_2, excessive hydrogen incorporation, led to a device becoming conductive, which results in the loss of switching characteristics. The evolution of μ_{lin} and V_{on} as a function of different GIs is presented in Figure S6. In addition, the defect passivation effect of hydrogen contributed to a substantial reduction in the level of hysteresis. The hysteresis results from charge trapping at the GI/OS interface or within the bulk GI.[33] During the forward and reverse V_G sweeps, these trapped charges affect current−voltage characteristics, ultimately causing hysteresis. In the PEALD supercycle process, increasing the number of H-rich SiO_2 cycles from 0 to 10 led to a decrease in the hysteresis from 1.13 to 0 V, suggesting improved stability as a result of hydrogen-induced trap passivation. Despite only a few more atomic layers increasing in the number of deposition cycles, the device characteristics exhibited significant variations. The devices with ten cycles of H-rich SiO_2, which was the optimum case for electrical characteristics, showed high mobility of ∼50 $cm^2/V{\cdot}s$ and appropriate values for S.S, V_{on}, and hysteresis and an on/off current ratio of $\sim 10^7$.

The value of μ_{FE} is calculated using

$$\mu_{lin} = \frac{g_m}{\frac{W}{L}\cdot C_i\cdot V_d} \qquad \left(\text{where } g_m \equiv \frac{\partial I_d}{\partial V_g}\right) \tag{1}$$

In addition, the value of V_{on} was calculated using

$$V_{on} = V_G \qquad \left(\text{where } I_D = 10pA \times \frac{W}{L}\right) \tag{2}$$

where W and L represent channel width and length, respectively, and C_i and k values of the GI provided in Figure S4. Breakdown voltage measurements (Figure S7) showed a slight decrease from 10.64 to 9.44 MV/cm with increasing number of H-rich SiO_2 cycles caused by the lower dielectric strength of SiO_2 compared to Al_2O_3. However, all devices maintained breakdown fields above 9 MV/cm, which confirms that the insulating reliability is not significantly affected.

The depth profiles of hydrogen and hydroxyl (OH) in film samples with the same stack sequence as the fabricated top-gate structured device are investigated using SIMS to confirm that the supercycle GI enables the refined control of H-related components (Figure 5a,b, respectively). Based on previous studies, hydrogen in OSs exists in multiple forms, including hydrogen interstitial bonding with oxygen (H_i^+), bonding with metal (H_i^-), combined with V_o (H_o^+), and the complex of V_o^0 + H_i^- ($H{-}DX^-$). Further, H_i^- and $H\text{-}DX^-$ exhibit deep impurity levels that act as electron traps and can influence device stability under bias and illumination.[28,50] In addition, in amorphous IZO, these deep levels are broadly distributed above the valence band maximum. In contrast, H_i^+ and H_o^+ are shallow states that act as electron donors to the host material. Given that hydrogen exists in various bonding states, distinguishing its specific configurations via SIMS remains challenging. However, SIMS analysis enables the detection of hydrogen species that function as electron donors, such as H_i^+ and H_O^+. The hydrogen H_O^+ detected in SIMS analysis is associated with V_o or incorporated within V_o sites.[20,50] Although partial overlap in depth profiles limited quantitative comparison, a subtle difference in hydrogen intensity can be discerned for devices with 10 and 15 cycles of H-rich SiO_2 compared with only the Al_2O_3 device, suggesting slightly enhanced hydrogen incorporation. However, a distinct quantitative variation in hydrogen concentration is not clearly observed in the H depth profiles. The observed increase in hydrogen intensity toward the back channel near the substrate is attributed to the interface effect in SIMS, which can artificially enhance signals at material boundaries rather than reflecting genuine hydrogen accumulation.[51]

H_i^+ is another hydrogen species that acts as a donor and can be analyzed in SIMS through OH intensity detection. In OSs, hydrogen bonding with oxygen results in OH formation. The reaction $H_i^+ + O^{2-} \rightarrow OH^- + e^-$ occurs when interstitial H interacts with weakly bonded oxygen in the semiconductor, generating OH and releasing free electrons, acting as a donor.[46,50,52,53] A slight increase in the OH concentration within the channel layer thickness was observed, and this trend

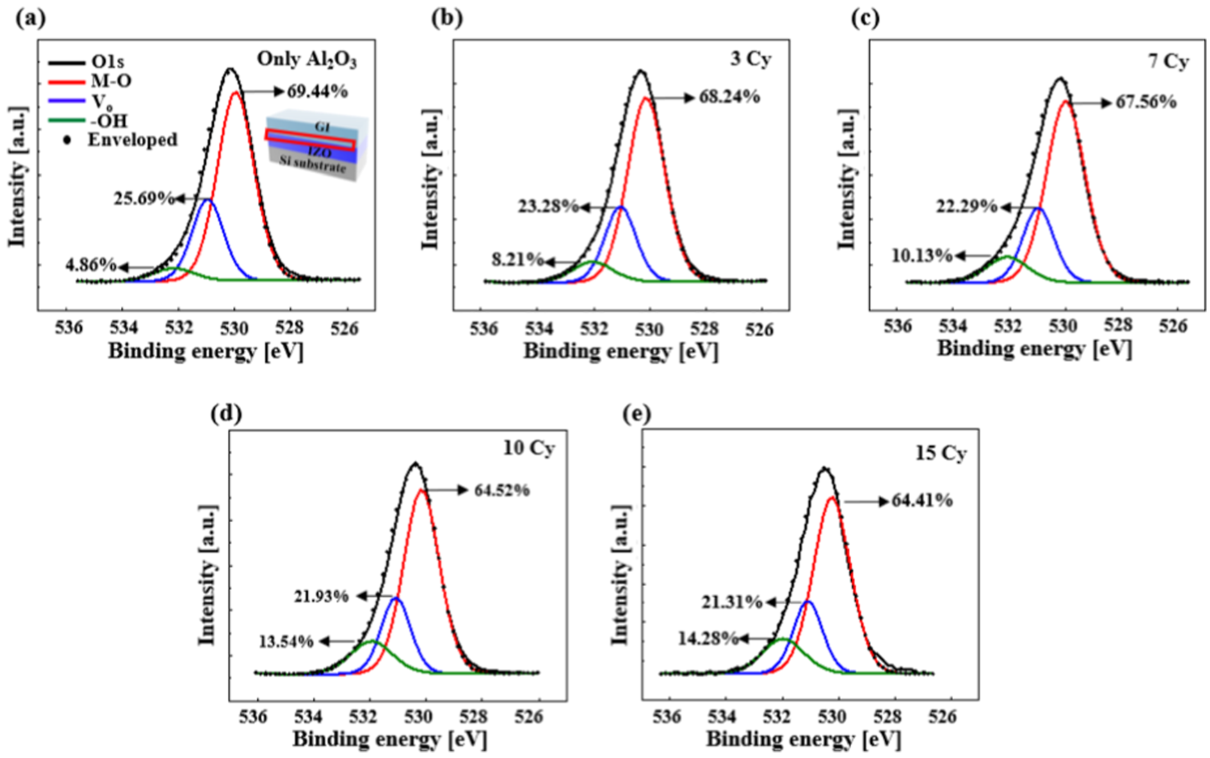

Figure 6. XPS O 1s spectra of the GI/IZO interface (a) with only Al$_2$O$_3$, (b) with 3 cycles of H-rich SiO$_2$, (c) with 7 cycles of H-rich SiO$_2$, (d) with 10 cycles of H-rich SiO$_2$, (e) with 15 cycles of H-rich SiO$_2$.

gradually intensified with an increasing number of H-rich SiO$_2$ cycles. These results indicate that hydrogen incorporated from the supercycled GI diffuses into the active layer, and it subsequently forms hydroxyl bonds with oxygen atoms, playing a critical role in determining the electrical properties of the TFTs. Due to the high-energy secondary ions used in SIMS measurement, existing bonds can be disrupted, making the detection of H$_o^+$ species weakly bound to V$_o$ sites challenging. In contrast, the bonding between O and H is considerably stronger than that of hydrogen in V$_o$ sites, resulting in clearer trends in the OH profiles. Consequently, variations in hydrogen incorporation are more prominent in the OH depth profiles than in the hydrogen profiles. Changes in OH concentrations in the channel region, as detected by SIMS, correlate with substantial improvements in electrical performance, including mobility enhancement and hysteresis reduction. Hydrogen within the OS contributes to free electron generation, increasing mobility via the percolation mechanism. In addition, hydrogen acts as a defect passivator by occupying V$_o$ sites ($H_i^+ + V_o \rightarrow H_o^+$),[50] which mitigates hysteresis effects. Such passivation further enhances both the mobility and device stability by eliminating trap sites that hinder electron flow. Even trace amounts of OH can significantly influence the electrical properties of high-mobility OSs, particularly in materials with high intrinsic carrier densities, as reflected by the pronounced performance variations in this study. Therefore, the precise control of hydrogen incorporation, as demonstrated by the PEALD supercycle process in this study, is crucial for optimizing oxide TFT performance.

Table 3. Proportions of Oxygen-Related Bonding States in IZO with Varying H-Rich SiO$_2$ Cycles in the GI

cycles of H-rich SiO$_2$ [cy]	M−O	oxygen vacancy	-OH
0 (only Al$_2$O$_3$)	69.44	25.69	4.86
3	68.24	23.28	8.21
7	67.56	22.29	10.13
10	64.52	21.93	13.54
15	64.41	21.31	14.28

To investigate the effect of hydrogen incorporation from varying cycles of H-rich SiO$_2$ on the oxygen bonding states at the near GI/OS interface region, XPS O 1s peak analysis was conducted using a depth-profile method on GI/OS stacked films, as shown in Figure 6a. This analysis is essential because the characteristics of OSs are strongly affected by their oxygen binding states.[54] Fabricated sample structures followed the TGBC process sequence to ensure an accurate representation of the actual device configurations. The O 1s spectra were deconvoluted into three components: metal−oxygen (M−O) bonding (530.4 ± 0.1 eV), oxygen vacancies (V$_o$, 531.4 ± 0.1 eV), and hydroxyl groups (OH, 532.5 ± 0.1 eV).[20] Figure 6 presents the O 1s spectra for devices with varying H-rich SiO$_2$ cycle counts 0, 3, 7, 10, and 15 cycles. The fractional contributions of each oxygen-related bond were determined by analyzing an area of the corresponding subpeaks and are summarized in Table 3. Although V$_o$ and O$_i$ are generally regarded as bulk-related defects, these species can contribute to charge trapping when located near the GI/OS interface. At the near GI/OS interface, V$_o$ can act as electron traps, which leads to charge trapping and potential device instability.[29] Further, in OSs, bulk O$_i$ acts as an electron trap, which can be passivated by hydrogen through the reaction $H^+ + O_i^{2-} \rightarrow OH + e^-$.[55] This passivation increases the OH content and elevates carrier concentration, which impacts the electrical properties of the oxide TFT. Hydrogen incorporation facilitated defect passivation with an increase in the number of H-rich SiO$_2$ cycles in the supercycled GI, effectively reducing the

https://doi.org/10.1021/acsami.5c12926
ACS Appl. Mater. Interfaces XXXX, XXX, XXX−XXX

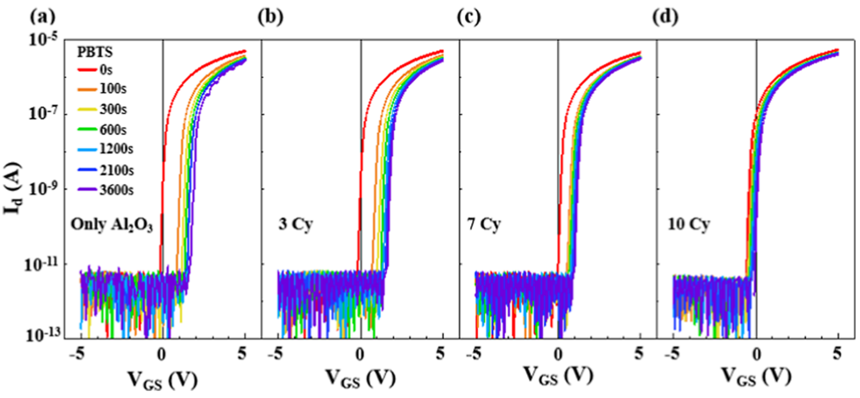

Figure 7. Transfer characteristics shifts induced by PBTS over time for TFTs with varying H-rich SiO_2 cycles: (a) with only Al_2O_3, (b) with 3 cycles of H-rich SiO_2, (c) with 7 cycles of H-rich SiO_2, (d) with 10 cycles of H-rich SiO_2.

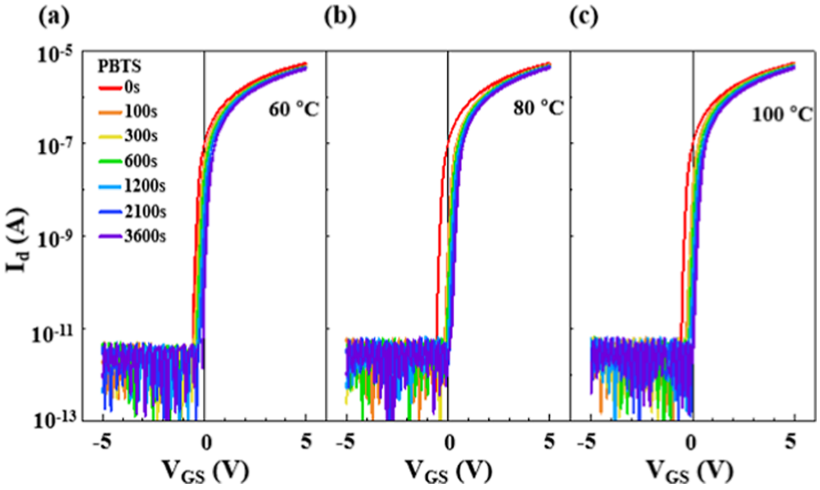

Figure 8. Transfer characteristics shifts induced by PBTS over time for TFTs with different temperature: (a) 60 °C, (b) 80 °C, (c) 100 °C.

concentration of oxygen vacancies and generating OH groups. Consequently, as the GI structure changed from only Al_2O_3 to a supercycled configuration with 15 cycles of H-rich SiO_2, the OH portion increased from 4.86% to 14.28%, which is consistent with the OH intensity trends observed in the SIMS depth profile. Simultaneously, the V_o content exhibited a decreasing trend from 25.69% to 21.31%, indicating the effective passivation of oxygen vacancies by hydrogen incorporation. Therefore, the XPS results confirm that the precise modulation of hydrogen incorporation through PEALD supercycle deposition enables controlled defect passivation at the GI/OS interface. To further confirm the reduction in total traps, the total trap density (N_T) was extracted using the following equation

$$N_T = N_{it} + N_{bulk} = \frac{C_i}{q}\cdot\left(\frac{S.\,S}{(\ln\ 10)kT/q} - 1\right) \qquad (3)$$

where N_{it} is the interfacial trap density, N_{bulk} is the bulk trap density, kT is the thermal energy, and q is the elementary charge.[45,56] The extracted N_T values exhibit a decreasing trend with increasing H-rich SiO_2 cycles, specifically 4.35×10^{11}, 3.70×10^{11}, 3.49×10^{11}, and 3.18×10^{11} $cm^{-2}\cdot eV^{-1}$ for 0, 3, 7, and 10 cycles, respectively. This reduction is consistent with the defect passivation suggested by hysteresis behavior and XPS and SIMS analyses. As this extraction is based on the S.S method and is included as a supplementary parameter, reflecting the overall trap passivation behavior. In addition, metal−insulator−semiconductor (MIS) $C-V$ measurements were performed at 1 MHz to analyze the trapped charge density ($Q_{trapped}$). Since the $Q_{trapped}$ is directly proportional to the hysteresis voltage (ΔV_{Hys}) in the $C-V$ curve, a reduction in ΔV_{Hys} indicates effective trap passivation.[57] As shown in Figure S8, ΔV_{Hys} systematically decreases with increasing number of H-rich SiO_2 cycles, confirming the progressive suppression of charge trapping and supporting the hydrogen-induced total trap passivation mechanism.

The positive bias temperature stability of the device can be explained using charge trapping modeling.[35,58] Under PBTS conditions, a positive shift in both the transfer curve and V_{on} occurs because of electron trapping at defect sites, including bulk defects within IZO, V_o, O_i, and dangling bonds at the GI/OS interface.[28] These defects act as charge trapping centers, which capture accumulated carriers and lead to device instability. The extent of the V_{on} shift is directly proportional to the frequency of charge trapping at these sites. This correlation highlights the critical role of defect passivation in improving the PBTS stability and overall device reliability. PBTS stability tests were performed under a bias condition of 1 MV at 60 °C for 3600 s[59,60] The transfer curves illustrating V_{on} shifts for each device are depicted in Figure 7.

A V_{on} shift of 1.8 V was observed in the device with only Al_2O_3 as the GI. For the device with three cycles of H-rich SiO_2, a V_{on} shift of 1.7 V occurred, while the device with seven cycles of H-rich SiO_2 showed a V_{on} shift of 1.1 V. The device with ten cycles of H-rich SiO_2 exhibited only a 0.5 V V_{on} shift, which indicates a significant reduction in the shift compared to that of the other devices. The extent of the positive shift in V_{on} decreases with an increase in the number of H-rich SiO_2 cycles, which indicates an improvement in the device stability. This enhancement in the PBTS stability is attributed to the passivation of defect states at the interface, where hydrogen atoms effectively interact with V_o sites and O_i, mitigating the effect of electron trapping. Extensive studies have investigated the role of hydrogen as a defect passivator and its influence on enhancing electrical stability.[31−33] Consequently, the incorporation of H-rich SiO_2 layers plays a crucial role in suppressing instability under prolonged positive bias stress conditions. Although the only Al_2O_3 device could also be further optimized by increasing the postannealing temperature (380 °C), achieving nearly zero hysteresis (Figure S9a), it still exhibited noticeable degradation under PBTS owing to residual defect-related trapping, as shown in Figure S9b.

Additional PBTS tests are conducted at varying temperatures (60, 80, and 100 °C) to further evaluate the stability of the device with ten cycles of H-rich SiO_2. Even at 100 °C, the device maintained stable electrical characteristics, exhibiting a V_{on} shift of only 0.6 V, as shown in Figure 8.

These results suggest that the passivation effect of H-rich SiO_2 effectively suppresses charge-trapping-induced instability, even under high-temperature conditions, confirming its role in enhancing PBTS stability without causing a normally on state.

Further, to evaluate stability under negative bias conditions, both the Negative Bias Temperature Test (NBTS) and Negative Bias Illumination Stress (NBIS) tests were performed. During NBTS, V_o act as hole trap centers, inducing a negative V_{on} shift.[61] In the device with ten cycles of H-rich SiO_2, the V_o sites were effectively passivated, and the inherently low hole density in n-type OSs further contributed to the negligible shift,[62] as shown in Figure S10a.

IZO channels are sensitive to illumination,[63] and deep hydrogen centers can undergo deep-to-shallow transitions under bias and thermal stress, introducing additional electrons into the conduction band and causing a negative V_{on} shift.[50] Therefore, the NBIS evaluation is essential for assessing device stability. Under NBIS, most devices exhibited negligible negative shifts, and even the device with ten cycles of H-rich SiO_2 exhibited only a minimal shift of 0.2 V (Figure S10b). This small change, attributed to a minor presence of deep hydrogen centers, indicates that precisely controlled hydrogen incorporation effectively suppresses NBIS degradation to a minimal level, ensuring that device stability under negative bias is largely maintained. While hydrogen incorporation is essential for shallow trap passivation and thus improves PBTS stability, its potential to cause slight NBIS degradation through deep-state formation underscores the importance of precise hydrogen control.

Furthermore, a constant current stress (CCS) test was conducted under bias conditions of $V_d = 3.5$ V and $V_g = 3.5$ V for 3000 s, corresponding to the saturation region. The output characteristics of the measured devices are illustrated in Figure S5. This measurement was used to evaluate the effect of on-state bias stress on device stability and to emulate the current-driven operating conditions of active-matrix organic light-emitting-diode pixel-driving TFTs. CCS serves as a complementary method to PBTS for assessing operational stability under simultaneous gate and drain bias. The reduction in drain current under this condition can lead to brightness variations in current-driven displays, and therefore, the normalized change in drain current is systematically analyzed. Figure 9 shows that the drain current decreased under the applied on-state bias, which was attributed to the screening effect of the gate bias caused by trapped charges.[22,64] The decay in on-current was modeled using a stretched exponential function expressed as

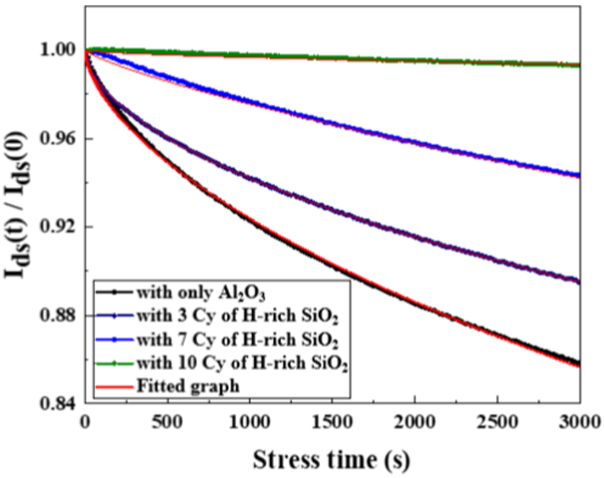

Figure 9. Decay of normalized drain current under CCS and corresponding fitted curves using a stretched exponential function.

$$\frac{I_D(t)}{I_D(0)} = \exp\left[-\left(\frac{t}{\tau}\right)^{\beta}\right] \tag{4}$$

where $I_D(0)$, β, and τ represent the initial state of the drain current ($t = 0$), dispersion parameter associated with the distribution of traps, and characteristic trapping time for electrons, respectively.[25,65] The red lines in Figure 9 correspond to fitting results based on eq 4. The device with ten cycles of H-rich SiO_2 exhibited the highest current retention of ∼99.97% after 3000 s, while the retention gradually declined to 94.3, 89.5, and 85.8% for devices with seven, three, and zero cycles, respectively. The values of fitting parameters τ and β are extracted from the fitted curve and are summarized in Table 4. TFT with ten cycles of H-rich SiO_2 exhibited a significantly higher value of τ compared to the TFTs with zero, three, and seven cycles of H-rich SiO_2. Therefore, the TFT with ten cycles of H-rich SiO_2 had significantly fewer trap sites.[66] The strong correlation between the experimental data and fitted curves confirms the stretched exponential behavior, indicating that charge trapping at defect sites is the primary mechanism responsible for these instabilities. This trend aligns well with prior PBTS stability data, indicating that hydrogen diffusion from the supercycled

Table 4. Extracted Characteristic Time for Trapping (τ) and Dispersion Parameters from the Current Decay Results

cycles of H-rich SiO_2 [cy]	τ [s]	β
0 (only Al_2O_3)	6.46×10^4	0.6078
3	1.02×10^5	0.5598
7	1.53×10^5	0.80
10	1.34×10^7	0.60

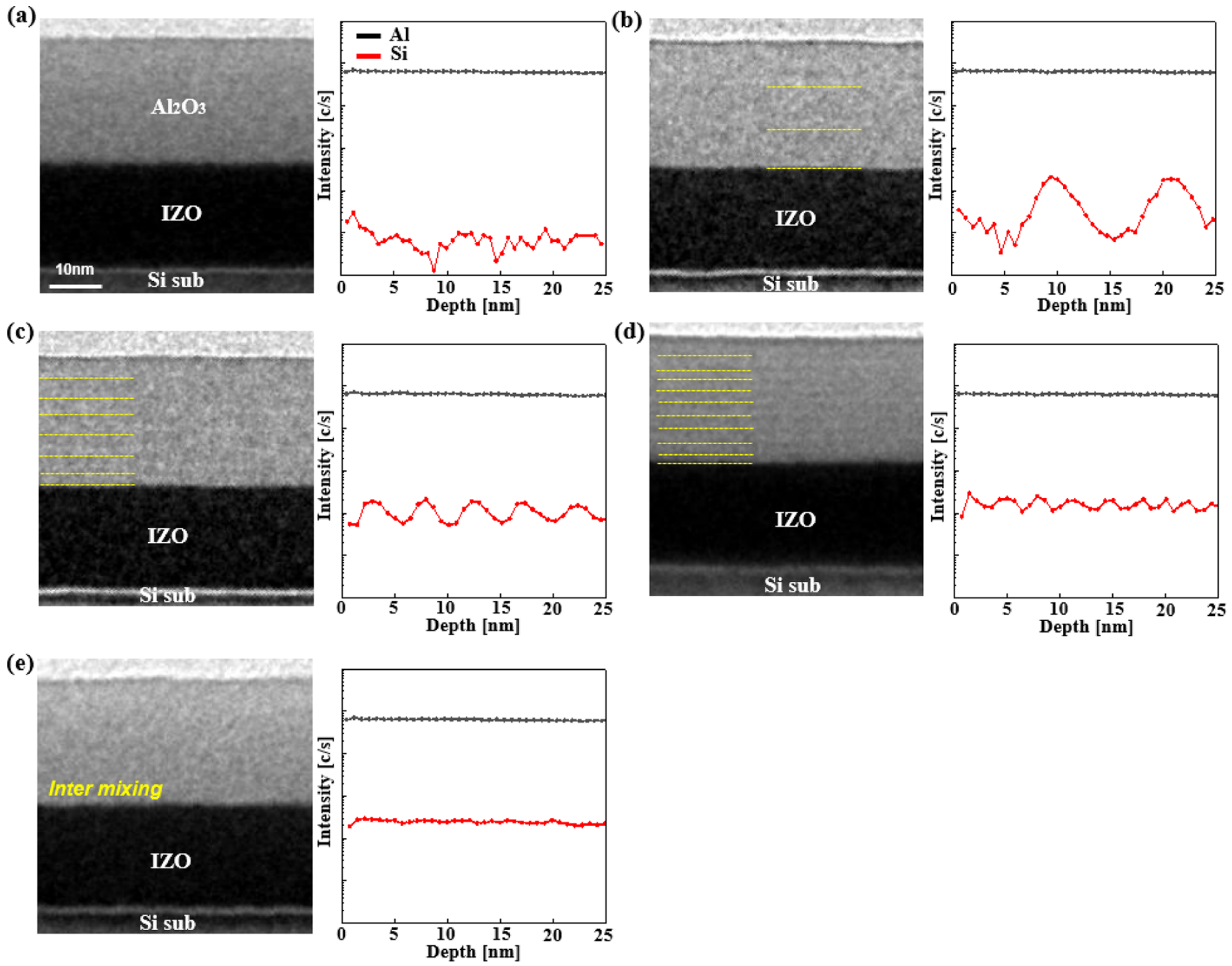

Figure 10. HRTEM images of cross-sectional film stacks with gate insulators and SIMS depth profiles at GI (a) with only Al_2O_3, (b) with 3 cycles of H-rich SiO_2, (c) with 7 cycles of H-rich SiO_2, (d) with 10 cycles of H-rich SiO_2, (e) with 15 cycles of H-rich SiO_2.

GI into the IZO channel and GI/OS interface plays a critical role in defect passivation by reducing trap sites. The device utilizing ten cycles of H-rich SiO_2 GI exhibited the most stable electrical characteristics and superior overall performance. This improvement is attributed to optimized hydrogen incorporation, which effectively passivated defect sites and maintained an optimized carrier concentration, minimizing the shift in the V_{on}.

As shown in Figure 10, HRTEM images of cross-sectional GI/OS stacks and SIMS depth profiles of the GI were analyzed for investigating the GI structure. Figure 10a−d present the GI structures of the H-rich SiO_2 and Al_2O_3 supercycle GIs with zero, three, seven, and ten cycles, respectively. The HRTEM images reveal a well-defined layered structure, whereas the corresponding SIMS depth profiles exhibit distinct Si peaks, suggesting the formation of alternating H-rich SiO_2 and Al_2O_3 layers. The repeating Al_2O_3 layers are considered to act as diffusion barriers for hydrogen transport. Prior studies reported that Al_2O_3 exhibits intrinsically lower hydrogen permeability and water vapor transmission rate compared to SiO_2, which suggests that the presence and arrangement of Al_2O_3 layers play a critical role in modulating hydrogen diffusion.[20,67] In the supercycle GI structure, two major changes occur with an increase in the number of H-rich SiO_2 cycles. The thickness of each repeating Al_2O_3 diffusion barrier layer decreases, effectively shortening the hydrogen diffusion path across the GI. Hydrogen accumulates more significantly near the GI/OS interface because of the increased number of H-rich SiO_2 insertions, which enhances hydrogen accessibility toward the active layer. These combined structural and compositional modifications promote the formation of more efficient hydrogen-related species transport pathways across the GI/OS interface and into the active layer, improving the electrical characteristics and stability of the fabricated TFTs. However, as shown in Figure 10 (e), the HRTEM image no longer reveals a layered structure in the case of 15 cycles. The SIMS profile shows no distinct Si peaks, indicating the formation of an intermixed morphology. This intermixing eliminates the discrete barrier effect of the Al_2O_3 layers and enables uncontrolled hydrogen diffusion. The excessive number of H-rich SiO_2 cycles leads to an overabundance of hydrogen supply, ultimately resulting in excessive carrier generation and a fully conductive channel state. In the HRTEM images of GI-only stacks (Figure S11), acquired at lower magnification to minimize high-energy beam exposure, distinct SiO_2 layers are more clearly visible for GI stacks with zero, three, seven, and ten cycles, whereas the 15 cycles sample exhibits intermixing between SiO_2 and Al_2O_3, consistent with the previous results.

The atomic force microscopy (AFM) measurements (Figure S12) confirm that the surface roughness of the GIs remains largely unchanged with an increase in the number of H-rich SiO_2 cycles. A slight increase in RMS roughness was observed for the device with 15 cycles of H-rich SiO_2, possibly due to increased intermixing at the GI surface. Nevertheless, the variation is minimal, indicating a negligible impact on the device performance.

Consequently, the SiO_2−Al_2O_3 supercycle approach enables precise control over hydrogen diffusion into the oxide channel by adjusting the number of supercycles during GI deposition. This strategy can be broadly applied to various OSs, offering a promising pathway to enhance the stability and performance of oxide TFTs.

4. CONCLUSION

We present a novel approach to precisely control hydrogen incorporation in top-gate oxide TFTs through a PEALD supercycled SiO_2−Al_2O_3 GI. This structure was developed to enable accurate control over hydrogen incorporation, simultaneously enhancing mobility and device stability. The hydrogen concentration in the OS channel was precisely tuned by modulating the number of H-rich SiO_2 cycles within the PEALD supercycle process. Systematic analyses including SIMS and XPS confirmed that the controlled hydrogen incorporation passivated oxygen-related defects such as oxygen vacancies and interstitial oxygen while contributing shallow donor states to increase carrier concentration. In addition, HRTEM and SIMS profiling verified the integrity of the layered GI structure and highlighted the role of Al_2O_3 as a diffusion barrier in regulating hydrogen transport. However, excessive hydrogen incorporation with 15 cycles of H-rich SiO_2 resulted in intermixing of the GI layers, leading to a loss of switching behavior and device degradation. CCS demonstrated a substantial suppression of charge trapping in the optimized device. The optimized device, fabricated with ten cycles of H-rich SiO_2, exhibited a high field-effect mobility of 47.4 $cm^2/V{\cdot}s$, zero hysteresis, an on/off ratio of $\sim 10^7$ and V_{on} shift of 0.5 V under PBTS at 60 °C, and remarkable stability under negative bias stress (negligible shift under NBTS and NBIS), underscoring the effectiveness of precise hydrogen control in enhancing both performance and stability. These results suggest that the SiO_2−Al_2O_3 supercycle approach provides a powerful platform for precise hydrogen control in various OS devices, enabling significant improvements in both performance and reliability.

■ ASSOCIATED CONTENT

Supporting Information

The Supporting Information is available free of charge at https://pubs.acs.org/doi/10.1021/acsami.5c12926.

> XRD pattern of the GI/IZO/Si stacks with 10 cycles of H-rich SiO_2; XPS depth profiles showing the atomic distribution of Al, In, O, Si, Zn, and C across the GI and active layer regions; SIMS depth profiles of all components in the GI; C−V curves of PEALD supercycle gate insulators with varying H-rich SiO_2 cycles; output curves of TFTs with PEALD supercycle gate insulators and transfer curve of the TFT with 10 cycles of H-rich SiO_2 measured at $V_d = 4.1$ V; changes in electric characteristics depending on varying H-rich SiO_2 cycles; Error bars represent the standard deviation obtained from measurements of 10 devices; breakdown characteristics of PEALD supercycle gate insulators with varying H-rich SiO_2 cycles; C−V characteristics of MIS capacitors with varying numbers of H-rich SiO_2 cycles measured at 1 MHz; optimized Only-Al_2O_3 device: transfer curve and PBTS characteristics; variation of transfer characteristics under NBTS at −1 MV/cm and 60 °C, and NBIS under light irradiation at 1 mW/cm^2 using a halogen lamp as the light source; HRTEM images of cross-sectional gate insulators; and AFM analysis of surface morphology of gate insulators with varying H-rich SiO_2 cycles in the PEALD supercycle structure (PDF)

■ AUTHOR INFORMATION

Corresponding Authors

Sang-Hee Ko Park − *Department of Materials Science and Engineering, Korea Advanced Institute of Science and Technology (KAIST), Daejeon 305-701, Republic of Korea;* orcid.org/0000-0001-7165-8211; Email: shkp@kaist.ac.kr

Jong Beom Ko − *Department of Materials Science and Engineering, Hanbat National University, Daejeon 34158, Republic of Korea;* orcid.org/0000-0002-0073-5918; Email: jko914@hanbat.ac.kr

Authors

Sunghwan Park − *Department of Materials Science and Engineering, Korea Advanced Institute of Science and Technology (KAIST), Daejeon 305-701, Republic of Korea;* orcid.org/0009-0007-5361-6684

Seong-In Cho − *Semiconductor R&D Center, Samsung Electronics Co., Ltd., Hwaseong-si 18448, Republic of Korea*

Hwa Young Kim − *Department of Materials Science and Engineering, Korea Advanced Institute of Science and Technology (KAIST), Daejeon 305-701, Republic of Korea*

Complete contact information is available at: https://pubs.acs.org/10.1021/acsami.5c12926

Author Contributions

S. H. Park: conceptualization, investigation, methodology, formal analysis, visualization, validation, writing original draft. S. I. Cho: Data curation, Conceptualization. H. Y. Kim: Data curation, investigation. Sang-Hee Ko Park and Jong Beom Ko: supervision, review and editing.

Notes

The authors declare no competing financial interest.

■ ACKNOWLEDGMENTS

This work was supported by the Technology Innovation Program (RS-2023-00231985, RS-2023-00235655) and NRF grant funded by the Korea government (MSIT) (No. RS-2023-00260527) and the Research Fund of Hanbat National University in 2024.

■ REFERENCES

(1) Nomura, K.; Ohta, H.; Takagi, A.; Kamiya, T.; Hirano, M.; Hosono, H. Room-Temperature Fabrication of Transparent Flexible Thin-Film Transistors Using Amorphous Oxide Semiconductors. *Nature* **2004**, *432* (7016), 488−492.

(2) Park, J. S.; Maeng, W.-J.; Kim, H.-S.; Park, J.-S. Review of Recent Developments in Amorphous Oxide Semiconductor Thin-Film Transistor Devices. *Thin Solid Films* **2012**, *520* (6), 1679−1693.

(3) Kwon, J. Y.; Son, K. S.; Jung, J. S.; Kim, T. S.; Ryu, M. K.; Park, K. B.; Yoo, B. W.; Kim, J. W.; Lee, Y. G.; Park, K. C.; Lee, S. Y.; Kim, J. M. Bottom-Gate Gallium Indium Zinc Oxide Thin-Film Transistor Array for High-Resolution AMOLED Display. *IEEE Electron Device Lett.* **2008**, *29* (12), 1309−1311.

(4) Kamiya, T.; Hosono, H. Material Characteristics and Applications of Transparent Amorphous Oxide Semiconductors. *NPG Asia Mater.* **2010**, *2* (1), 15−22.

(5) Belmonte, A.; Oh, H.; Rassoul, N.; Donadio, G. L.; Mitard, J.; Dekkers, H.; Delhougne, R.; Subhechha, S.; Chasin, A.; Van Setten, M. J.; Kljucar, L.; Mao, M.; Puliyalil, H.; Pak, M.; Teugels, L.; Tsvetanova, D.; Banerjee, K.; Souriau, L.; Tokei, Z.; Goux, L.; Kar, G. S. Capacitor-Less, Long-Retention (>400s) DRAM Cell Paving the Way towards Low-Power and High-Density Monolithic 3D DRAM. *2020 IEEE International Electron Devices Meeting (IEDM)*; IEEE: San Francisco, CA, USA, 2020, pp 28.2.1−28.2.4.

(6) Li, Z.; Wu, J.; Mei, X.; Huang, X.; Saraya, T.; Hiramoto, T.; Takahashi, T.; Uenuma, M.; Uraoka, Y.; Kobayashi, M. A 3D Vertical-Channel Ferroelectric/Anti-Ferroelectric FET With Indium Oxide. *IEEE Electron Device Lett.* **2022**, *43* (8), 1227−1230.

(7) Yan, G.; Yang, H.; Liu, W.; Zhou, N.; Hu, Y.; Shi, Y.; Gao, J.; Tian, G.; Zhang, Y.; Fan, L.; Wang, G.; Xu, G.; Bi, J.; Yin, H.; Zhao, C.; Luo, J. Mechanism Analysis of Ultralow Leakage and Abnormal Instability in InGaZnO Thin-Film Transistor Toward DRAM. *IEEE Trans. Electron Devices* **2022**, *69* (5), 2417−2422.

(8) Jeong, S.; Jang, S.; Han, H.; Kim, H.; Choi, C. C-Axis Aligned Crystalline Indium-Gallium-Zinc Oxide (CAAC-IGZO) and High-k Charge Trapping Film for Flash Memory Application. *J. Alloys Compd.* **2021**, *888*, 161440.

(9) Nakagawa, T.; Negoro, Y.; Yoneda, S.; Shishido, H.; Kobayashi, H.; Oota, M.; Kawata, T.; Ikeda, T.; Yamazaki, S. Image Sensor with In-Pixel Calculation Using Crystalline IGZO FET in Display. *Jpn. J. Appl. Phys.* **2020**, *59* (SG), SGGE01.

(10) Hur, J. S.; Lee, S.; Moon, J.; Jung, H.-G.; Jeon, J.; Yoon, S. H.; Park, J.-H.; Jeong, J. K. Oxide and 2D TMD Semiconductors for 3D DRAM Cell Transistors. *Nanoscale Horiz.* **2024**, *9* (6), 934−945.

(11) Sheng, J.; Hong, T.; Lee, H.-M.; Kim, K.; Sasase, M.; Kim, J.; Hosono, H.; Park, J.-S. Amorphous IGZO TFT with High Mobility of 70 Cm^2/(V s) via Vertical Dimension Control Using PEALD. *ACS Appl. Mater. Interfaces* **2019**, *11* (43), 40300−40309.

(12) Shi, Y.; Shiah, Y.-S.; Sim, K.; Sasase, M.; Kim, J.; Hosono, H. High-Performance a-ITZO TFTs with High Bias Stability Enabled by Self-Aligned Passivation Using a-GaOx. *Appl. Phys. Lett.* **2022**, *121* (21), 212101.

(13) Huang, T.; Liu, H.; Fan, C.; Zhou, X.; Zhang, S. 30.3: Impact of Top Gate Insulator Deposition Temperature on Electrical Performance of Dual-Gate a-InZnO TFTs. *SID Symp. Dig. Tech. Pap.* **2023**, *54* (S1), 206−208.

(14) Cho, S.-I.; Jeon, J. B.; Kim, J. H.; Lee, S. H.; Jeong, W.; Kim, J.; Kim, G.; Kim, K. M.; Park, S.-H. K. Synaptic Transistors with Human Brain-like fJ Energy Consumption *via* Double Oxide Semiconductor Engineering for Neuromorphic Electronics. *J. Mater. Chem. C* **2021**, *9* (32), 10243−10253.

(15) Lee, C.-H.; Yoo, K. S.; Kim, D.-G.; Park, C.-K.; Park, J.-S. Compositionally Engineered Amorphous InZnO Thin-Film Transistor with High Mobility and Stability via Atmospheric Pressure Spatial Atomic Layer Deposition. *J. Ind. Eng. Chem.* **2024**, *140*, 269−276.

(16) Fortunato, E.; Barquinha, P.; Pimentel, A.; Pereira, L.; Gonçalves, G.; Martins, R. Amorphous IZO TTFTs with Saturation Mobilities Exceeding 100 Cm^2/Vs. *Phys. Status Solidi RRL* **2007**, *1* (1), R34.

(17) Moreira, M.; Carlos, E.; Dias, C.; Deuermeier, J.; Pereira, M.; Barquinha, P.; Branquinho, R.; Martins, R.; Fortunato, E. Tailoring IGZO Composition for Enhanced Fully Solution-Based Thin Film Transistors. *Nanomaterials* **2019**, *9* (9), 1273.

(18) Kim, H. W.; Kim, E. S.; Park, J. S.; Lim, J. H.; Kim, B. S. Influence of Effective Channel Length in Self-Aligned Coplanar Amorphous-Indium-Gallium-Zinc-Oxide Thin-Film Transistors with Different Annealing Temperatures. *Appl. Phys. Lett.* **2018**, *113* (2), 022104.

(19) Park, J. C.; Lee, H.-N.; Im, S. Self-Aligned Top-Gate Amorphous Indium Zinc Oxide Thin-Film Transistors Exceeding Low-Temperature Poly-Si Transistor Performance. *ACS Appl. Mater. Interfaces* **2013**, *5* (15), 6990−6995.

(20) Ko, J. B.; Cho, S.-I.; Park, S.-H. K. Engineering a Subnanometer Interface Tailoring Layer for Precise Hydrogen Incorporation and Defect Passivation for High-End Oxide Thin-Film Transistors. *ACS Appl. Mater. Interfaces* **2023**, *15* (40), 47799−47809.

(21) Choi, C. H.; Kim, T.; Ueda, S.; Shiah, Y.-S.; Hosono, H.; Kim, J.; Jeong, J. K. High-Performance Indium Gallium Tin Oxide Transistors with an Al_2 O_3 Gate Insulator Deposited by Atomic Layer Deposition at a Low Temperature of 150 °C: Roles of Hydrogen and Excess Oxygen in the Al_2 O_3 Dielectric Film. *ACS Appl. Mater. Interfaces* **2021**, *13* (24), 28451−28461.

(22) Cho, S.-I.; Ko, J. B.; Lee, S. H.; Kim, J.; Park, S.-H. K. Remarkably Stable High Mobility Self-Aligned Oxide TFT by Investigating the Effect of Oxygen Plasma Time during PEALD of SiO2 Gate Insulator. *J. Alloys Compd.* **2022**, *893*, 162308.

(23) Kim, D.-G.; Yoo, K. S.; Kim, H.-M.; Park, J.-S. Impact of N_2 O Plasma Reactant on PEALD-SiO_2 Insulator for Remarkably Reliable ALD-Oxide Semiconductor TFTs. *IEEE Trans. Electron Devices* **2022**, *69* (6), 3199−3205.

(24) Kim, D.-G.; Choi, H.; Kim, Y.-S.; Lee, D.-H.; Oh, H.-J.; Lee, J. H.; Kim, J.; Lee, S.; Kuh, B.; Kim, T.; Kim, H. Y.; Park, J.-S. Selectively Nitrogen Doped ALD-IGZO TFTs with Extremely High Mobility and Reliability. *ACS Appl. Mater. Interfaces* **2023**, *15* (26), 31652−31663.

(25) Ko, J. B.; Lee, S.-H.; Park, K. W.; Park, S.-H. K. Interface Tailoring through the Supply of Optimized Oxygen and Hydrogen to Semiconductors for Highly Stable Top-Gate-Structured High-Mobility Oxide Thin-Film Transistors. *RSC Adv.* **2019**, *9* (62), 36293−36300.

(26) Kim, H. W.; Oh, C.; Jang, H.; Kim, M. Y.; Kim, B. S. Influence of Oxygen-Related Defects on In-Ga-Sn-O Semiconductor Due to Plasma-Enhanced Atomic Layer Deposition of Al2O3 for Low-Temperature Thin-Film Transistor in Terms of Electrical Properties. *J. Alloys Compd.* **2022**, *918*, 165649.

(27) Barquinha, P.; Pereira, L.; Gonçalves, G.; Martins, R.; Fortunato, E.; Kuscer, D.; Kosec, M.; Vilà, A.; Olziersky, A.; Morante, J. R. Low-temperature Sputtered Mixtures of High-κ and High Bandgap Dielectrics for GIZO TFTs. *J. Soc. Inf. Disp.* **2010**, *18* (10), 762−772.

(28) Hong, H.; Kim, M. J.; Yi, D.-J.; Shin, D. Y.; Moon, Y.-K.; Son, K.-S.; Lim, J. H.; Jeong, K.; Chung, K.-B. Quantitative Dynamic Evolution of Unoccupied States in Hydrogen Diffused InGaZnSnO TFT under Positive Bias Temperature Stress. *ACS Appl. Electron. Mater.* **2024**, *6* (10), 7584−7590.

(29) Han, W. H.; Oh, Y. J.; Chang, K. J.; Park, J.-S. Electronic Structure of Oxygen Interstitial Defects in Amorphous In-Ga-Zn-O Semiconductors and Implications for Device Behavior. *Phys. Rev. Appl.* **2015**, *3* (4), 044008.

(30) Trinh, T. T.; Nguyen, V. D.; Ryu, K.; Jang, K.; Lee, W.; Baek, S.; Raja, J.; Yi, J. Improvement in the Performance of an InGaZnO Thin-Film Transistor by Controlling Interface Trap Densities between the Insulator and Active Layer. *Semicond. Sci. Technol.* **2011**, *26* (8), 085012.

(31) Hanyu, Y.; Domen, K.; Nomura, K.; Hiramatsu, H.; Kumomi, H.; Hosono, H.; Kamiya, T. Hydrogen Passivation of Electron Trap in Amorphous In-Ga-Zn-O Thin-Film Transistors. *Appl. Phys. Lett.* **2013**, *103* (20), 202114.

(32) Kim, M.-H.; Park, J.; Lim, J.-H.; Choi, D.-K. The Effect of Hydrogen on the Device Stability of Amorphous InGaZnO Thin-Film Transistors under Positive Bias with Various Temperature Stresses. *Phys. Status Solidi A* **2019**, *216* (20), 1900297.

(33) Nam, Y.; Kim, H.-O.; Cho, S. H.; Hwang, C.-S.; Kim, T.; Jeon, S.; Ko Park, S.-H. Beneficial Effect of Hydrogen in Aluminum Oxide Deposited through the Atomic Layer Deposition Method on the Electrical Properties of an Indium−Gallium−Zinc Oxide Thin-Film Transistor. *J. Inf. Disp.* **2016**, *17* (2), 65−71.

(34) Han, K.-L.; Ok, K.-C.; Cho, H.-S.; Oh, S.; Park, J.-S. Effect of Hydrogen on the Device Performance and Stability Characteristics of Amorphous InGaZnO Thin-Film Transistors with a SiO2/SiNx/SiO2 Buffer. *Appl. Phys. Lett.* **2017**, *111* (6), 063502.

(35) Jeong, J. K.; Won Yang, H.; Jeong, J. H.; Mo, Y.-G.; Kim, H. D. Origin of Threshold Voltage Instability in Indium-Gallium-Zinc Oxide Thin Film Transistors. *Appl. Phys. Lett.* **2008**, *93* (12), 123508.

(36) Noh, H. Y.; Kim, J.; Kim, J.-S.; Lee, M.-J.; Lee, H.-J. Role of Hydrogen in Active Layer of Oxide-Semiconductor-Based Thin Film Transistors. *Crystals* **2019**, *9* (2), 75.

(37) Lee, Y.; Nam, T.; Seo, S.; Yoon, H.; Oh, I.-K.; Lee, C. H.; Yoo, H.; Kim, H. J.; Choi, W.; Im, S.; Yang, J. Y.; Choi, D. W.; Yoo, C.; Kim, H.; Kim, H. Hydrogen Barriers Based on Chemical Trapping Using Chemically Modulated Al_2 O_3 Grown by Atomic Layer Deposition for InGaZnO Thin-Film Transistors. *ACS Appl. Mater. Interfaces* **2021**, *13* (17), 20349−20360.

(38) Abliz, A. Effects of Hydrogen Plasma Treatment on the Electrical Performances and Reliability of InGaZnO Thin-Film Transistors. *J. Alloys Compd.* **2020**, *831*, 154694.

(39) Kim, H. Y.; Cho, S.-I.; Shin, D. Y.; Chung, K.-B.; Park, S.-H. K.; Ko, J. B. Optimized Hydrogen-Supplying Gate Insulator for High-Mobility Indium Oxide TFTs via Atomic-Level Oxygen Reactant Engineering. *J. Alloys Compd.* **2025**, *1020*, 179353.

(40) Zhao, Y.; Liu, J.; Hua, Z.; Jin, L.; Huo, Z. Influence of BEOL Process on Poly-Si Grain Boundary Traps Passivation in 3D NAND Flash Memory. *Solid-State Electron.* **2019**, *156*, 28−32.

(41) Wang, B.; Gao, B.; Wu, H.; Qian, H. A Drain Leakage Phenomenon in Poly Silicon Channel 3D NAND Flash Caused by Conductive Paths along Grain Boundaries. *Microelectron. Eng.* **2018**, *192*, 66−69.

(42) Lee, S.; Kang, Y.-H.; Kim, M.-S.; Lee, H.; Cho, Y.-H.; Kim, M.; Yoon, T.-S.; Kim, H.-M.; Kim, K.-B. Effect of the Bilayer Period of Atomic Layer Deposition on the Growth Behavior and Electrical Properties of the Amorphous In−Zn−O Film. *ACS Appl. Mater. Interfaces* **2020**, *12* (35), 39372−39380.

(43) Gonçalves, G.; Elangovan, E.; Barquinha, P.; Pereira, L.; Martins, R.; Fortunato, E. Influence of Post-Annealing Temperature on the Properties Exhibited by ITO, IZO and GZO Thin Films. *Thin Solid Films* **2007**, *515* (24), 8562−8566.

(44) Kim, Y.; Hwang, T.; Oh, H.; Park, J. S.; Park, J. Reliability Engineering of High-Mobility IGZO Transistors via Gate Insulator Heterostructures Grown by Atomic Layer Deposition. *Adv. Mater. Interfaces* **2024**, *11* (15), 2301097.

(45) Kim, T.; Nam, Y.; Hur, J.; Park, S.-H. K.; Jeon, S. The Influence of Hydrogen on Defects of In−Ga−Zn−O Semiconductor Thin-Film Transistors With Atomic-Layer Deposition of Al_2 O_3. *IEEE Electron Device Lett.* **2016**, *37* (9), 1131−1134.

(46) Cho, S.-I.; Woo, N.; Jeong, H.-J.; Park, S.-H. K. Inserting Interfacial Layer for Atomic-Scaled Hydrogen Control to Enhance Electrical Properties of InZnO TFTs. *IEEE Electron Device Lett.* **2023**, *44* (4), 650−653.

(47) Sheng, J.; Han, J.-H.; Choi, W.-H.; Park, J.; Park, J.-S. Performance and Stability Enhancement of In−Sn−Zn−O TFTs Using SiO_2 Gate Dielectrics Grown by Low Temperature Atomic Layer Deposition. *ACS Appl. Mater. Interfaces* **2017**, *9* (49), 42928−42934.

(48) Van De Walle, C. G. Hydrogen as a Cause of Doping in Zinc Oxide. *Phys. Rev. Lett.* **2000**, *85* (5), 1012−1015.

(49) Wang, H.; He, J.; Xu, Y.; André, N.; Zeng, Y.; Flandre, D.; Liao, L.; Li, G. Impact of Hydrogen Dopant Incorporation on InGaZnO, ZnO and In_2 O_3 Thin Film Transistors. *Phys. Chem. Chem. Phys.* **2020**, *22* (3), 1591−1597.

(50) Kang, Y.; Ahn, B. D.; Song, J. H.; Mo, Y. G.; Nahm, H.; Han, S.; Jeong, J. K. Hydrogen Bistability as the Origin of Photo-Bias-Thermal Instabilities in Amorphous Oxide Semiconductors. *Adv. Electrode Mater.* **2015**, *1* (7), 1400006.

(51) Toda, T.; Wang, D.; Jiang, J.; Hung, M. P.; Furuta, M. Quantitative Analysis of the Effect of Hydrogen Diffusion from Silicon Oxide Etch-Stopper Layer into Amorphous In−Ga−Zn−O on Thin-Film Transistor. *IEEE Trans. Electron Devices* **2014**, *61* (11), 3762−3767.

(52) Kamiya, T.; Nomura, K.; Hosono, H. Origins of High Mobility and Low Operation Voltage of Amorphous Oxide TFTs: Electronic Structure, Electron Transport, Defects and Doping. *J. Disp. Technol.* **2009**, *5* (7), 273−288.

(53) Noh, H. Y.; Lee, W.-G.; G, R. H.; Cha, J.-H.; Kim, J.-S.; Yun, W. S.; Lee, M.-J.; Lee, H.-J. Hydrogen Diffusion and Its Electrical Properties Variation as a Function of the IGZO Stacking Structure. *Sci. Rep.* **2022**, *12* (1), 19816.

(54) Nomura, K.; Kamiya, T.; Ikenaga, E.; Yanagi, H.; Kobayashi, K.; Hosono, H. Depth Analysis of Subgap Electronic States in Amorphous Oxide Semiconductor, a-In-Ga-Zn-O, Studied by Hard x-Ray Photoelectron Spectroscopy. *J. Appl. Phys.* **2011**, *109* (7), 073726.

(55) Bae, S.-H.; Yang, J.-H.; Kim, Y.-H.; Kwon, Y. H.; Seong, N.-J.; Choi, K.-J.; Hwang, C.-S.; Yoon, S.-M. Roles of Oxygen Interstitial Defects in Atomic-Layer Deposited InGaZnO Thin Films with Controlling the Cationic Compositions and Gate-Stack Processes for the Devices with Subμm Channel Lengths. *ACS Appl. Mater. Interfaces* **2022**, *14* (27), 31010−31023.

(56) Yang, Z.; Yang, J.; Meng, T.; Qu, M.; Zhang, Q. Influence of Channel Layer Thickness on the Stability of Amorphous Indium Zinc Oxide Thin Film Transistors. *Mater. Lett.* **2016**, *166*, 46−50.

(57) Lin, J.; Gomeniuk, Y. Y.; Monaghan, S.; Povey, I. M.; Cherkaoui, K.; O'Connor, E. ´.; Power, M.; Hurley, P. K. An Investigation of Capacitance-Voltage Hysteresis in Metal/High- *k*/In0.53Ga0.47As Metal-Oxide-Semiconductor Capacitors. *J. Appl. Phys.* **2013**, *114* (14), 144105.

(58) Xu, P.-R.; Yao, R.-H. Threshold-Voltage Shift Model Based on Electron Tunneling under Positive Gate Bias Stress for Amorphous InGaZnO Thin-Film Transistors. *Displays* **2018**, *53*, 14−17.

(59) Yoo, K. S.; Lee, C.-H.; Kim, D.-G.; Choi, S.-H.; Lee, W.-B.; Park, C.-K.; Park, J.-S. High Mobility and Productivity of Flexible In2O3 Thin-Film Transistors on Polyimide Substrates via Atmospheric Pressure Spatial Atomic Layer Deposition. *Appl. Surf. Sci.* **2024**, *646*, 158950.

(60) Kim, J.; Kim, D. H.; Cho, S.-I.; Lee, S. H.; Jeong, W.; Park, S.-H. K. Channel-Shortening Effect Suppression of a High-Mobility Self-Aligned Oxide TFT Using Trench Structure. *IEEE Electron Device Lett.* **2021**, *42* (12), 1798−1801.

(61) Jeong, J.; Lee, G. J.; Kim, J.; Kim, J.; Choi, B. Oxygen Dispersive Diffusion Induced Bias Stress Instability in Thin Active Layer Amorphous In−Ga−Zn−O Thin-Film Transistors. *Appl. Phys. Express* **2013**, *6* (3), 031101.

(62) Lee, S.; Nathan, A.; Jeon, S.; Robertson, J. Oxygen Defect-Induced Metastability in Oxide Semiconductors Probed by Gate Pulse Spectroscopy. *Sci. Rep.* **2015**, *5* (1), 14902.

(63) Barquinha, P.; Pimentel, A.; Marques, A.; Pereira, L.; Martins, R.; Fortunato, E. Effect of UV and Visible Light Radiation on the Electrical Performances of Transparent TFTs Based on Amorphous Indium Zinc Oxide. *J. Non-Cryst. Solids* **2006**, *352* (9−20), 1756−1760.

(64) Singh, S.; Mohapatra, Y. N. Bias Stress Effect in Solution-Processed Organic Thin-Film Transistors: Evidence of Field-Induced Emission from Interfacial Ions. *Org. Electron.* **2017**, *51*, 128−136.

(65) Lee, J.-M.; Cho, I.-T.; Lee, J.-H.; Kwon, H.-I. Bias-Stress-Induced Stretched-Exponential Time Dependence of Threshold Voltage Shift in InGaZnO Thin Film Transistors. *Appl. Phys. Lett.* **2008**, *93* (9), 093504.

(66) Lee, W. H.; Choi, H. H.; Kim, D. H.; Cho, K. 25th Anniversary Article: Microstructure Dependent Bias Stability of Organic Transistors. *Adv. Mater.* **2014**, *26* (11), 1660−1680.

(67) Choi, W.-H.; Kim, K.; Jeong, S.-G.; Han, J.-H.; Jang, J.; Noh, J.; Park, K.-S.; Kim, J.-J.; Yoon, S.-Y.; Jeon, W.; Park, J.-S. The Significance on Structural Modulation of Buffer and Gate Insulator for ALD Based InGaZnO TFT Applications. *IEEE Trans. Electron Devices* **2021**, *68* (12), 6147−6153.